A GENERAL FRAMEWORK FOR CONSISTENT ESTIMATION OF CHARGE TRANSPORT PROPERTIES VIA RANDOM WALKS IN RANDOM ENVIRONMENTS[*]

OLE STENZEL[†], CHRISTIAN HIRSCH[†], TIM BRERETON[†], BJOERN BAUMEIER[‡], DENIS ANDRIENKO[‡], DIRK KROESE[§], AND VOLKER SCHMIDT[†]

Abstract. A general framework is proposed for the study of the charge transport properties of materials via random walks in random environments (RWRE). The material of interest is modeled by a random environment, and the charge carrier is modeled by a random walker. The framework combines a model for the fast generation of random environments that realistically mimic materials morphology with an algorithm for efficient estimation of key properties of the resulting random walk. The model of the environment makes use of tools from spatial statistics and the theory of random geometric graphs. More precisely, the disordered medium is represented by a random spatial graph with directed edge weights, where the edge weights represent the transition rates of a Markov jump process (MJP) modeling the motion of the random walker. This MJP is a multiscale stochastic process. In the long term, it explores all vertices of the random graph model. In the short term, however, it becomes trapped in small subsets of the state space and makes many transitions in these small regions. This behavior makes efficient estimation of velocity by Monte Carlo simulations a challenging task. Therefore, we use aggregate Monte Carlo (AMC), introduced in [T. Brereton et al., *Methodol. Comput. Appl. Probab.*, 16 (2014), pp. 465–484], for estimating the velocity of a random walker as it passes through a realization of the random environment. In this paper, we prove the strong consistency of the AMC velocity estimator and use this result to conduct a detailed case study, in which we describe the motion of holes in an amorphous mesophase of an organic semiconductor, dicyanovinyl-substituted oligothiophene (DCV4T). In particular, we analyze the effect of system size (i.e., number of molecules) on the velocity of single charge carriers.

1. Introduction. Random walks in random environments (RWRE) are fundamental models in many branches of the physical sciences (see, for example, [11]). Generally, the random environment models a disordered system, and the random walker represents the motion of a single particle through this system. The RWRE formalism allows for the study of numerous mathematically and physically interesting properties of disordered systems. Continuous time versions of these random walks are

[†]Institute of Stochastics, Ulm University, 89069 Ulm, Germany (ole.stenzel@uni-ulm.de, christian. hirsch@uni-ulm.de, timothy.brereton@uni-ulm.de, volker.schmidt@uni-ulm.de). The second author kindly acknowledges support by a research grant from DFG Research Training Group 1100 at Ulm University.

[‡]Max Planck Institute for Polymer Research, 55128 Mainz, Germany (baumeier@mpip-mainz. mpg.de, denis.andrienko@mpip-mainz.mpg.de).

[§]School of Mathematics and Physics, The University of Queensland, Brisbane 4072, Australia (kroese@maths.uq.edu.au). This author acknowledges the support of the Australian Research Council under grant DP0985177.

particularly important in materials science, where they provide a basis for the study of the transport properties of materials. Much of the discussion of RWRE has focused on mathematically tractable models, often in infinite settings (e.g., [31]). These models have been very successful in describing important physical phenomena. In practice, however, it is often necessary to consider more complex environments. An example is when the morphology of an organic semiconductor plays an important role in determining charge transport characteristics.

The main quantity of interest when studying charge transport is the average velocity with which charges traverse the random environment at a given external field (inducing a drift to the charges), which corresponds to charge mobility when normalized by the field. A key feature of many RWRE is the presence of "traps" in the random environment, where the random walker becomes stuck for long periods of time. These traps have a significant impact on the average velocity of the random walker. In addition, trap regions present considerable difficulties in obtaining numerical solutions of the Markov jump process (MJP) modeling the random walk. This is because the resulting stochastic process is effectively multiscale. At long timescales, the random walker moves between trap regions, exploring the state space. At short timescales, the walker moves about within trap regions. In the theory of numerical solutions of (embedded) Markov chains, such processes are said to have the property of being *nearly completely decomposable.*

In this paper, we propose a novel framework to study charge transport properties of materials via random walkers in disordered random media. This framework combines a stochastic model for the fast generation of random environments that realistically models materials morphology with an algorithm for efficient estimation of key properties of the resulting random walk. This algorithm, called aggregate Monte Carlo (AMC), was originally introduced in [5] and is a method for estimating the velocity of a random walker as it passes through a realization of the random environment. The algorithm works by first identifying, and then aggregating, problem regions in the random environment. We show that we are able to do this in such a way that our estimator is strongly consistent. Our stochastic morphology model represents the disordered medium as a random spatial graph with directed edge weights, where the edge weights represent the transition rates of an MJP modeling the motion of the random walker, and extends the spatial graph model introduced in [2]. It makes use of tools from spatial statistics and the theory of random geometric graphs. A particular strength is that it allows efficient simulation of large-scale molecular systems.

We then present our methodology. We describe a model of an example which illustrates an amorphous mesophase of an organic dye, used as an electron-donor in organic solar cells; see Figure 1. Here, the random environment represents a molecular morphology, and the random walker describes the movement of a charge (hole) through the morphology. More specifically, we adjust the parameters of the model to the electronic properties of dicyanovinyl-substituted oligothiophene (DCV4T) molecules in a small (microscopic) system. The fitted model can be used to predict the mobility of holes in a morphology of DCV4T molecules. Such a model can be of use for better understanding solar cells, as it allows for larger-scale (experimentally relevant) modeling of such microscopic structures.

The stochastic approach presented here is not limited to the particular organic semiconductor (DCV4T) we have used as a test system. In fact, the majority of host materials in organic light emitting diodes have large energetic disorder (deep traps) and are therefore challenging to model using small systems and the conventional variable step size method; see [16, 17, 20]. Stochastic modeling helps to increase the
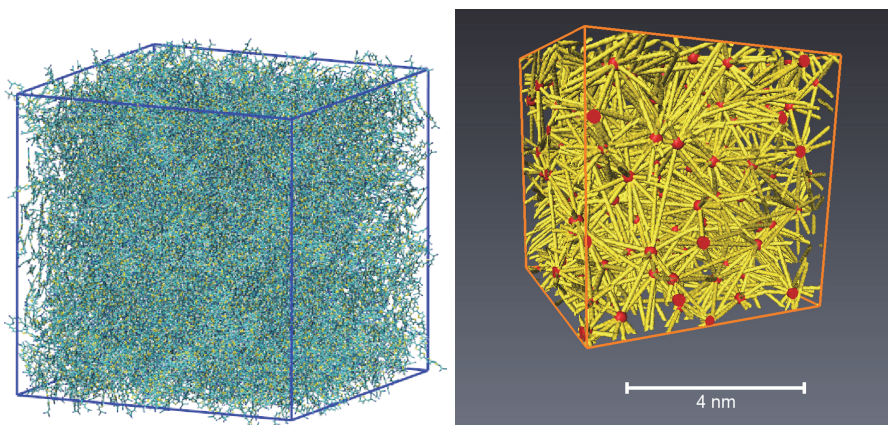
FIG. 1. *Left: Large-scale morphology of DCV4T gained by microscopic simulations. Right: corresponding three-dimensional (3D) graph extracted from DCV4T morphology (cut-out), where vertices are displayed in red and edges are marked in yellow.*

size of the system, while AMC provides an efficient way of evaluating its properties, e.g., charge carrier mobility. Moreover, the developed techniques are not restricted to organic semiconductors. Similar problems are encountered, for example, when studying surface reactions (catalysis) (see [12]) or hydrogen and oxygen transport in biological systems (see [30]).

The paper is organized as follows. In section 2, we introduce our model of random environments. Section 3 deals with estimation of the random walker's velocity, describing the standard estimation technique and the AMC approach. We give a proof that the AMC provides a strongly consistent estimator of the random walker's velocity. In section 4, we use our framework to analyze charge transport properties of DCV4T molecules for a number of different realizations of the stochastic morphology model and different system sizes. Conclusions are given in section 5.

2. A stochastic model of disordered media. The random environment that we propose is a random spatial graph with directed edge weights, where the edge weights describe the transition rates of an MJP governing the motion of the random walker. This model has been designed primarily as a tool for the study of charge transport. However, note that the graph model introduced in the following has numerous other potential applications (see, e.g., [11, Chapter 5]).

The random graph model consists of spatially distributed random vertices and random weighted edges. More precisely, the random geometric graph can be described by a triple $G = (V, E, W)$, with V being the set of random vertices, E the set of random edges, and W the set of random edge weights. We divide our modeling approach for the random three-dimensional (3D) graph G into three parts: the modeling of the set of vertices, the modeling of the set of edges, and the modeling of the set of edge weights. The procedure for generating the graph (without edge weights) is illustrated in Figure 2.

As stated above, this model has been designed primarily as a tool for charge transport studies. In this context, note that every material system in the real world is of finite spatial extent. The active layer of an organic solar cell, for instance, consists of a blend of electron-donor (e.g., DCV4T) and electron-acceptor molecules and has a thickness of around 100–200 nm. Thus, it is reasonable to simulate a
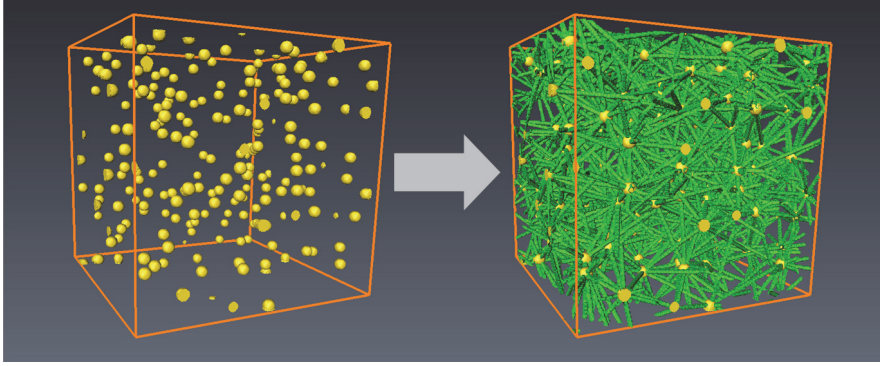
FIG. 2. *The first two stages in generating the random environment model. First, the vertices are generated using the dominance-competition model (left). Second, the edges are placed according to the model detailed in section 2.3 (right).*

random environment not in an infinite but in a finite setting. Therefore, the random graph model will be simulated in a bounded (cubic) observation window $A = [0, a_x] \times [0, a_y] \times [0, a_z] \subset \mathbb{R}^3$, $a_x, a_y, a_z > 0$. In particular, in our case study (see section 4), we analyze the effect of system size (i.e., the volume of A) on the transport properties of single charges. It turns out that the system size has a significant effect on transport properties. Although we define the stochastic morphology model for bounded, cubic observation windows, the model could be defined on $\mathbb{R}^3$. In particular, if defined on $\mathbb{R}^3$, the model has the properties of stationarity and isotropy which allow the application of important structural (point process and image) characteristics. Restricting a model to a bounded observation window means that boundary effects may be an issue. In this paper, we avoid boundary effects by imposing cyclic boundary conditions (see section 2.1). This essentially means changing the distance metric, as explained below.

2.1. Cyclic boundary conditions. We impose cyclic boundary conditions as follows. More precisely, we measure the signed x, y, and z distances between two vertices, $s_i = (x_i, y_i, z_i)$ and $s_j = (x_j, y_j, z_j)$, by

$$(2.1) \qquad \mathbf{d}_{s_i, s_j} = \left(d_{s_i, s_j}^x, d_{s_i, s_j}^y, d_{s_i, s_j}^z \right)^\mathsf{T},$$

where

$$(2.2) \qquad d_{s_i, s_j}^x = \begin{cases} x_j - x_i & \text{if } |x_j - x_i| \leq a_x/2, \\ a_x + (x_j - x_i) & \text{if } |x_j - x_i| > a_x/2 \text{ and } x_i > x_j, \\ -a_x + (x_j - x_i) & \text{if } |x_j - x_i| > a_x/2 \text{ and } x_i < x_j, \end{cases}$$

and $d_{s_i, s_j}^y, d_{s_i, s_j}^z$ are defined analogously. We can then introduce the metric

$$(2.3) \qquad \delta(s_i, s_j) = \sqrt{\left(d_{s_i, s_j}^x \right)^2 + \left(d_{s_i, s_j}^y \right)^2 + \left(d_{s_i, s_j}^z \right)^2}.$$

2.2. The vertex model. To model the vertex set V of the graph G, we use the dominance-competition model (see [26]), which is based on a thinning of a Poisson point process in $\mathbb{R}^3$. The dominance-competition model, adapted for the simulation in a bounded observation window A, can be described as follows: first, a set of points,

$\{\xi_k\}_{k=1}^{L^0}$, is generated, where the points are independent and uniformly distributed in A, given the total number of points, L^0, which follows a Poisson distribution with parameter $\lambda \cdot \nu_3(A)$, with $\nu_3(A)$ being the volume of A. We refer to λ as being the intensity (average number of points per volume unit) of the random set of points $\{\xi_k\}_{k=1}^{L^0}$. Each point ξ_k is assigned a ball $B(\xi_k, R_k)$ with midpoint ξ_k and a random radius $R_k \sim \mathsf{Gamma}(\iota_{\mathsf{mean}}, \iota_{\mathsf{var}}) + r_h$, where $r_h > 0$. We then thin the set $\{\xi_k\}_{k=1}^{L^0}$ as follows. A point ξ_k is retained only if there does not exist another point, ξ_j, such that $\xi_k \in B(\xi_j, R_j)$ and the volume of $B(\xi_j, R_j)$ is bigger than the volume of $B(\xi_k, R_k)$. The random set of remaining points, $\{S_i\}_{i=1}^{L}$, where L is the total number of remaining points, is called a dominance-competition process; see [26] for more details. Note that each "surviving" point S_i has a distance of at least $R_i \geq r_h$ from its nearest neighbor. For any fixed parameters ι_{mean}, ι_{var}, and r_h of the radii distribution, the maximum intensity that can be obtained by this point process model is limited (see, for example, [7] for the case in which $R_i = r_h$). The intensity, however, can be increased by further iterations. More specifically, in each step a dominance-competition process is generated independently of all preceding processes. Points from this new process are added to the existing process provided that they do not "interact" with any existing points (i.e., they are not included in the sphere of any existing point and no existing point is included in their sphere). See [2] for more details. The dominance-competition model has a broad range of applications. This is because it provides a large degree of control over many important properties of point processes.

1. The intensity can be adjusted by changing λ, the intensity of the underlying Poisson process. Large intensities can be obtained by further iterations of the dominance-competition process.
2. The hard-core distance r_h sets a minimum distance between neighboring points. This is important because particles cannot overlap in most physical models (e.g., grains and molecules).
3. The distribution of the distances between points can be controlled by changing the parameters ι_{mean} and ι_{var} of the Gamma distribution and the hard-core distance r_h.
4. It is possible to adjust the degree of regularity. A highly ordered point process can be obtained by combining a high intensity (optionally by applying further iterations of the dominance-competition process) with a large hard-core distance and a Gamma distribution with small variance. In contrast, a more disordered point process can be obtained by increasing the variance of the Gamma distribution.

This model is parsimonious but captures the "hard-core" nature of molecules and allows considerable control over the degree of regularity of the point process (which is important when modeling irregular systems). Models with fewer parameters were considered but were unable to combine a flexible distribution for the distances between centers of mass with sufficient control over the regularity of the resulting system. The parsimony of the model means that it is relatively easy to fit to experimental data. In addition, dominance-competition point processes are stationary and isotropic if defined on the entirety of $\mathbb{R}^3$, allowing the use of many important point process characteristics; see section 4.2.

2.3. The edge model. Given a set of vertices $V = \{s_i\}_{i=1}^{\ell}$, we place edges between neighboring vertices to generate a 3D spatial graph. The edge model, presented

in the following, has four important features:

1. Edges are placed between all sufficiently close vertices: those less than r_{min} apart.
2. No edges are placed between vertices that are more than r_{max} distant from one another.
3. The probability of an edge being put between two vertices decreases as the distance between the vertices increases.
4. In so far as possible, a minimum vertex degree of d_{min} is obtained.

These features allow considerable control over the connectivity properties of the graph.

ALGORITHM 2.1 (edge placement algorithm). *For each vertex, $s_i \in V$, do the following.*

1. *Find $\mathcal{N}_i^{\mathsf{max}} = \{j \in \mathbb{N} : s_j \in V \setminus \{s_i\}$ and $\delta(s_i, s_j) < r_{\mathsf{max}}\}$.*
2. *Find $\mathcal{N}_i^{\mathsf{min}} = \{j \in \mathbb{N} : s_j \in V \setminus \{s_i\}$ and $\delta(s_i, s_j) < r_{\mathsf{min}}\}$. Place edges between s_i and all $s_j, j \in \mathcal{N}_i^{\mathsf{min}}$. Put $\mathcal{N}_i^{\mathsf{rem}} = \mathcal{N}_i^{\mathsf{max}} \setminus \mathcal{N}_i^{\mathsf{min}}$. Let $K_i = |\mathcal{N}_i^{\mathsf{min}}|$. If $K_i \geq d_{\mathsf{min}}$, go to step 4.*
3. *Let $M_i = |\mathcal{N}_i^{\mathsf{max}}|$. If $M_i < d_{\mathsf{min}}$, then connect s_i to all the remaining nearest neighbors less than r_{max} away, and terminate the algorithm. Otherwise, place $d_{\mathsf{min}} - K_i$ edges between s_i and vertices in $\mathcal{N}_i^{\mathsf{rem}}$. This is done as follows.*
   i. *Set $k = 0$.*
   ii. *Select a vertex $s_j, j \in \mathcal{N}_i^{\mathsf{rem}}$, with probability $\frac{f(\delta(s_i, s_j))}{\sum_{l \in \mathcal{N}_i^{\mathsf{rem}}} f(\delta(s_i, s_l))}$, where $f : [0, \infty) \to [0, 1]$ is a suitably chosen, monotonically decreasing function.*
   iii. *Place an edge between s_j and s_i, set $\mathcal{N}_i^{\mathsf{rem}} = \mathcal{N}_i^{\mathsf{rem}} \setminus \{j\}$, and set $k = k+1$.*
   iv. *If $k \geq d_{\mathsf{min}} - K_i$, terminate. Otherwise, go to step ii.*
4. *Put an edge between s_i and each remaining $s_j, j \in \mathcal{N}_i^{\mathsf{rem}}$, with probability $\alpha_{i,j}$, where*

$$\alpha_{i,j} = \min\left(1, \frac{cf(\delta(s_i, s_j))}{\sum_{l \in \mathcal{N}_i^{\mathsf{rem}}} f(\delta(s_i, s_l))}\right).$$

The parameter $c > 0$ controls the average number of edges being added.

2.4. The edge weight model. The set of directed edge weights W is generated according to the high-temperature limit of nonadiabatic transfer (Marcus theory; see [15]) with the transfer rate given by

$$(2.4) \qquad w_{ij} = \frac{2\pi}{\hbar} \frac{\mathcal{J}_{ij}^2}{\sqrt{4\pi\lambda_{ij}k_{\mathrm{B}}T}} \exp\left[-\frac{(\Delta\eta_{ij} - \lambda_{ij})^2}{4\lambda_{ij}k_{\mathrm{B}}T}\right],$$

where T is the temperature, $\hbar$ the reduced Planck constant, and k_{B} Boltzmann's constant. The quantities on the right-hand side of (2.4) that are specific to pairs of vertices are the reorganization energy, λ_{ij}, the electronic coupling element (or transfer integral), $\mathcal{J}_{ij}$, and the energy difference, $\Delta\eta_{ij} = \Delta\eta^{\mathsf{el}} + \Delta\eta^{\mathsf{ext}}$. The energy difference consists of the difference in electrostatic site-energies, $\Delta\eta^{\mathsf{el}} = \eta_i - \eta_j$, and the influence of an externally applied electric field $\mathbf{F} \in \mathbb{R}^3$, $\Delta\eta^{\mathsf{ext}} = q\langle\mathbf{F}, \mathbf{d}_{s_i, s_j}\rangle$, where q is the charge of the carrier and $\langle\,,\,\rangle$ denotes the scalar product.

In this paper, we model the two most important pair-specific components: electrostatic site-energies η_i and electronic coupling elements J_{ij}. The reorganization energy, λ_{ij}, is taken to be constant.

In charge transport, transfer rates depend exponentially on energy differences between neighboring molecules. A key feature is that the energy of each molecule

is strongly positively correlated with the energies of neighboring molecules. To reproduce these correlations, we use a flexible moving-average–type model for these energies. In addition, we model the distribution of electronic coupling elements between molecules. Given the molecular energies and the electronic coupling elements, we are able to calculate transfer rates using (2.4).

We associate an energy η_i to each vertex s_i. The $\{\eta_i\}_{i=1}^{\ell}$ are generated according to a process similar to that used by [2]. We generate two independent sequences of independent and $\mathsf{N}(0, \sigma_\eta^2)$-distributed random variables, $\{\epsilon_i\}_{i=1}^{\ell}$ and $\{\widetilde{\epsilon}_i\}_{i=1}^{\ell}$. Let

$$\mathcal{N}_i^k = \left\{ j_1, \ldots, j_k \in \{1, \ldots, \ell\} : \max_{k \in \{1, \ldots, k\}} \delta(s_{j_k}, s_i) \leq \min_{l \in \{1, \ldots, \ell\} \setminus \{j_1, \ldots, j_k\}} \delta(s_l, s_i) \right\}$$

be the indices of the k nearest neighbors of vertex s_i (including index i). Then, we set

$$(2.5) \qquad \eta_i = \sqrt{\omega}\epsilon_i + \sqrt{\frac{1 - \omega}{k}} \sum_{j \in \mathcal{N}_i^k} \widetilde{\epsilon}_j + \mu_\eta \quad , \quad i = 1, \ldots, \ell,$$

where $\mu_\eta > 0$ is a constant chosen to fit empirical data. The number K controls the range of the spatial correlation, and the weight $\omega \in [0, 1]$ controls the magnitude of the spatial correlation. The resulting energies, $\{\eta_i\}_{i=1}^{\ell}$, are $\mathsf{N}(\mu_\eta, \sigma_\eta^2)$-distributed with the desired correlation structure.

Roughly speaking, the electronic coupling elements, $\{\mathcal{J}_{ij}\}_{i=1, j=1, i \neq j}^{\ell, \ell}$, describe the quality of the connections between molecules. The quality of the connection between a molecule at s_i and a neighboring molecule at s_j is highly dependent on the distance between the two vertices. We model the squared electronic coupling elements as log-normal random variables with parameters that are distance dependent. That is, for each i and j, $i \neq j$, we set $\mathcal{J}_{ij}^2 = \exp\{X_{ij}\}$, where $X_{ij} \sim \mathsf{N}\left(\mu_{\mathcal{J}}(\delta(s_i, s_j)), \sigma_{\mathcal{J}}^2(\delta(s_i, s_j))\right)$. Both $\mu_{\mathcal{J}}(\cdot)$ and $\sigma_{\mathcal{J}}^2(\cdot)$ are polynomial functions. For $i = j$, we set $\mathcal{J}_{ij} = 0$.

If an edge exists between s_i and s_j, then the weights between them are given by $w_{ij} > 0$ and $w_{ji} > 0$ as defined in (2.4). Otherwise $w_{ij} = w_{ji} = 0$. Note that the random geometric graph constructed in this way is connected, as unconnected realizations are rejected.

3. Aggregate Monte Carlo. A fundamental quantity in charge transport is the charge mobility. This corresponds to the average velocity of a charge carrier under the influence of an external electric field normalized by the magnitude of the field. The difficulty in calculating charge mobility lies in calculating the velocity of the charge carrier. In our case, this corresponds to calculating the velocity of a random walker in the appropriately chosen random environment. The continuous time random walk approach which directly describes the microscopic motion of carriers was pioneered in [21] and [22] (see also [18]).

Tractable closed form expressions for the velocity of random walkers in random environments are only available for very simple models. In complex models, such as that presented above, the velocity must be estimated statistically. In order to estimate the velocity, a realization or a number of realizations of the stochastic morphology model is generated, and Monte Carlo simulations are performed by simulating random walks on these realizations. The two algorithms we describe for estimating charge mobility do not rely on a particular shape of the density of states (DOS) but on rates

only. This means the algorithms are generally applicable and can be used for any DOS. Time, field, and temperature dependencies all enter the rates and are fully incorporated into all resulting calculations.

A key feature of RWRE models is that the velocity of the random walker tends to be slower than it would be in an equivalent environment without random distribution of energies. This is because of the presence of energetic traps in which the random walker becomes stuck for long periods of time. In the charge transport context, these regions can be thought of as "valleys" in the energy surface. These traps present significant difficulties to the estimation of random walker velocity, as the random walker exhibits multiscale dynamics: over larger timescales it moves between trap regions; over shorter timescales it moves about within trap regions. In many cases, the MJP governing the motion of the random walker is nearly completely decomposable. An MJP with this characteristic causes a number of numerical difficulties; see the discussion in [6]. In particular, when the random environment is large, many standard techniques for computational solutions of Markov chains fail (see, e.g., [25]).

We have developed an algorithm, AMC, that is particularly efficient in estimating the velocity of random walks in environments with traps (see [5]). It uses aggregation techniques similar to those used to approximate steady state solutions to nearly completely decomposable Markov chains: problem regions are aggregated into single states in such a manner that the velocity estimator remains consistent. Because velocity is a quantity that is much more dependent on the long-run dynamics of the MJP than it is on the short-run dynamics, this estimator gives considerable efficiency gains over standard techniques. It is important to stress that this estimator does not result in any loss of information when calculating charge mobility, as all pertinent information is preserved during the aggregation step. In particular, the AMC algorithm does not reduce the system size or replace multiple states with single states, whose sojourn times are approximated by exponential random variables. Instead, we replace a stochastic process on the fine state space (an MJP) with a qualitatively different process on the coarsened state space (a discrete time Markov chain). This second process completely captures the long-run properties of the original MJP. In the case of estimating charge mobility, we make this explicit by providing a proof of consistency; see Theorems 3.1 and 3.2.

We begin by describing the standard process by which the velocity of a continuous time random walker is estimated, either for a realization of a random environment model, as above, or for a completely deterministic environment. We call this approach, used extensively in the physics literature (see, for example, [27, 29]), the *crude Monte Carlo* (CMC) approach.

3.1. Crude Monte Carlo.

3.1.1. CMC estimator for the velocity. Consider a finite connected graph with directed edge weights, $G = (V, E, W)$, in the bounded window A. We take the edge weights to be the transition rates of an MJP, $M = \{M_t\}_{t \geq 0}$, with state space V. We set $\ell = |V|$ and label the vertices from 1 to ℓ; that is, we identify vertex s_i with state i for $i \in \{1, \ldots, \ell\}$. The generator matrix $\{q_{i,j}\}_{i,j \in V}$ of the MJP is given by $q_{i,j} = w_{ij}$ for $i \neq j$ and $q_{i,i} = -q_i = -\sum_{j \neq i} q_{i,j}$. We define $\widetilde{M} = \{\widetilde{M}_n\}_{n \geq 0}$ to be the embedded Markov jump chain whose transition matrix is denoted by $J = \{p_{i,j}\}_{i,j \in V}$, with $p_{i,j} = q_{i,j}/q_i, i \neq j$. The associated sequence of waiting times is given by $\{T_n\}_{n \geq 0}$. Let N_t be the random number of transitions up to time $t > 0$.

The average velocity of the random walker is the vector quantity defined by

$$(3.1) \qquad \mathbf{v} = \lim_{t\to\infty} \frac{1}{t} \sum_{n=0}^{N_t-1} \mathbf{d}_{\widetilde{M}_n,\widetilde{M}_{n+1}}.$$

We will see later that the limit in (3.1) exists almost surely (a.s.) and, moreover, that $\mathbf{v}$ is a.s. constant given the weighted graph $G = (V, E, W)$. This immediately gives the following natural estimator of the velocity:

$$(3.2) \qquad \widehat{\mathbf{v}_{\mathsf{cmc}}}(t) = \frac{1}{t} \sum_{n=0}^{N_t-1} \mathbf{d}_{\widetilde{M}_n,\widetilde{M}_{n+1}}.$$

This estimator is straightforward to implement in the bounded window A.

ALGORITHM 3.1 (crude Monte Carlo (CMC) estimation of velocity).
1. *Select $\widetilde{M}_0$ uniformly from $1,\ldots,\ell$. Put $t = 0$ and $\mathbf{d} = \mathbf{0}$. Put $n = 0$.*
2. *Put $\widetilde{M}_{n+1} = i$ with probability $q_{\widetilde{M}_n,i}/q_{\widetilde{M}_n}$.*
3. *Put $t = t + \tau$, where $\tau \sim \mathsf{Exp}(q_{\widetilde{M}_n})$.*
4. *Put $\mathbf{d} = \mathbf{d} + \mathbf{d}_{\widetilde{M}_n,\widetilde{M}_{n+1}}$.*
5. *Put $n = n + 1$, and repeat from step 2 until $t > t_0$.*
6. *Return the estimator $\widehat{\mathbf{v}_{\mathsf{cmc}}}(t) = \mathbf{d}/t$.*

3.1.2. Asymptotic properties of the CMC estimator. Note that the MJP M is irreducible, as we require our graph to be connected, so there exists a unique stationary limiting distribution $\boldsymbol{\pi} = \{\pi_i\}_{i=1}^{\ell}$. This yields an alternative definition of the velocity in terms of the stationary distribution of the random walker that is used in the following asymptotic result.

THEOREM 3.1. *Let $\tilde{\mathbf{v}} = \sum_{s,s'\in V} \pi_s q_{s,s'} \mathbf{d}_{s,s'}$. Then $\mathbf{v} = \lim_{t\to\infty} \widehat{\mathbf{v}_{\mathsf{cmc}}}(t) = \tilde{\mathbf{v}}$ a.s. and in L^1.*

The velocity $\tilde{\mathbf{v}}$ defined above has the following heuristic interpretation. Asymptotically, the fraction of time the MJP M spends in state $s \in V$ is given by π_s. When the walker is in state s it moves to state $s' \in V$ at the infinitesimal rate $q_{s,s'}$ with an associated displacement vector given by $\mathbf{d}_{s,s'}$. This yields an instantaneous velocity of $q_{s,s'}\mathbf{d}_{s,s'}$. Averaging these velocities over all possible transitions results in the expression $\tilde{\mathbf{v}} = \sum_{s,s'\in V} \pi_s q_{s,s'} \mathbf{d}_{s,s'}$.

Note that Theorem 3.1 follows easily from the standard ergodic theorem for MJPs [19, Theorem 3.8.1]. Some minor complications arise from the observations that the sum in (3.2) is associated with the (embedded) jump chain, while the average in (3.2) is considered in the continuous time variable t and in that the distances appearing in (3.2) have to be considered as functionals of a related bivariate Markov chain. To be more precise, in order to apply the ergodic theorem for MJPs it is convenient to consider the intermediate estimator

$$\mathbf{v}_{\mathsf{c},1}(t) = \frac{1}{t} \sum_{s,s'\in V} T_{s,s'}(t) q_{s'} \mathbf{d}_{s,s'}, \qquad t > 0,$$

where $T_{s,s'}(t)$ denotes the time the MJP M spends in state s' with state s being the previously visited state. That is, for $s, s' \in V$,

$$T_{s,s'}(t) = \nu_1\left(t' \in [0,t] : \widetilde{M}_{N_{t'}-1} = s, \widetilde{M}_{N_{t'}} = s'\right),$$

where ν_1 is the one-dimensional Lebesgue measure. In the appendix we show that

$$\lim_{t\to\infty} (\widehat{\mathbf{v}_{\mathsf{cmc}}}(t) - \mathbf{v}_{\mathsf{c},1}(t)) = 0$$

with probability 1; see Lemma A.1.

Next, we show that $\mathbb{P}\left(\lim_{t\to\infty} \mathbf{v}_{\mathsf{c},1}(t) = \tilde{\mathbf{v}}\right) = 1$. For this purpose it is convenient to introduce the bivariate process $M^{\mathsf{sub}} = \left(M_{1,t}^{\mathsf{sub}}, M_{2,t}^{\mathsf{sub}}\right)_{t\geq 0}$ defined by $M_{1,t}^{\mathsf{sub}} = \widetilde{M}_{N_t-1}$ and $M_{2,t}^{\mathsf{sub}} = \widetilde{M}_{N_t}$. Here we choose $\widetilde{M}_{-1}$ to be an arbitrary neighbor of $\widetilde{M}_0$. Then M^{sub} forms an irreducible MJP on the subset V^{sub} of V^2 consisting of those $(s,s') \in V^2$ with $q_{s,s'} > 0$. We denote the stationary limit distribution of M^{sub} by $\{\pi_{(s,s')}^{\mathsf{sub}}\}_{(s,s')\in V^{\mathsf{sub}}}$ and observe that the ergodic theorem for MJPs (see [19, Theorem 3.8.1]) implies

$$(3.3) \qquad \mathbb{P}\left(\lim_{t\to\infty} \mathbf{v}_{\mathsf{c},1}(t) = \sum_{(s,s')\in V^{\mathsf{sub}}} \pi_{(s,s')}^{\mathsf{sub}} q_{s'} \mathbf{d}_{s,s'}\right) = 1.$$

In order to represent $\pi_{(s,s')}^{\mathsf{sub}} q_{s'} \mathbf{d}_{s,s'}$ in terms of the stationary distribution of the original chain $(\widetilde{M}_n)_{n\geq 0}$, we first note that the generator $(q_{(s,s'),(s',s'')}^{\mathsf{sub}})_{(s,s'),(s',s'')\in V^{\mathsf{sub}}}$ of M^{sub} is determined by $q_{(s,s'),(s',s'')}^{\mathsf{sub}} = q_{s',s''}$ for $s' \neq s''$. Hence, for every $(s',s'') \in V^{\mathsf{sub}}$,

$$\sum_{s\in V\setminus\{s'\}} \pi_s q_{s,s'} q_{(s,s'),(s',s'')}^{\mathsf{sub}}/q_{s'} = \sum_{s\in V\setminus\{s'\}} \pi_s q_{s,s'} q_{s',s''}/q_{s'} = \pi_{s'} q_{s',s''} = \frac{\pi_{s'} q_{s',s''}}{q_{s''}} q_{(s,s'')}^{\mathsf{sub}}.$$

Additionally, $\sum_{(s,s')\in V^{\mathsf{sub}}} \pi_s q_{s,s'}/q_{s'} = \sum_{s'\in V} \pi_{s'} = 1$, so that $\pi_{(s,s')}^{\mathsf{sub}} = \pi_s q_{s,s'}/q_{s'}$. This completes the proof of the a.s. convergence in Theorem 3.1. The proof of L^1-convergence is provided in the appendix (see Lemma A.2).

3.2. AMC. The CMC estimator performs very poorly in many settings (see, for example, [5]). This is because the realizations of the random environment can contain traps in which the walker becomes stuck. The walker then spends a very large number of steps moving around in a small region before it is able to escape and explore more of the environment. Simulating all of these steps is computationally very expensive. However, because velocity is a long-run quantity, its value is largely unaffected by the short-run behavior of the random walker within trap regions. The idea of the AMC algorithm is to replace these traps with single states so that the random walker can explore the entire random environment much more rapidly. Because the expected time spent in each problem region and the probabilities of moving into and out of problem regions can be calculated exactly, this procedure results in a velocity estimator that is strongly consistent. In comparative studies (see [5] and [6]), this estimator has been found to be between 100 and 1000 times faster than the CMC estimator (that is, to achieve equally accurate answers using CMC, a sample size 100 to 1000 times larger would be required).

The AMC approach consists of three steps:

1. Identifying the problem regions in a given environment.
2. Aggregating these problem regions into single states.
3. Carrying out a simulation of the random walk on the resulting coarsened environment.

3.2.1. Identifying the problem regions. We wish to define a partition $\{V_j\}_{j=1}^{\mathcal{L}}$ of the state space V, such that traps in the original state space are contained within

single elements of the new partition, where $\mathcal{L}$ denotes the number of "superstates." In order to identify the problem regions in the state space, we consider the embedded jump chain $\widetilde{M}$. This is because the computational cost of simulating the random walker depends not on the physical time spent in each state but rather on the number of transitions between states required to adequately explore the state space. The problem regions are regions within which the walker moves with high probability but from which it escapes with low probability. The walker quickly reaches almost stationarity within these regions but takes much longer to reach stationarity over the whole environment.

We use a clustering algorithm given in [8] for partitioning nearly completely decomposable Markov chains. Consider the weighted directed graph $\widetilde{G} = (\widetilde{V}, \widetilde{E}, \widetilde{W})$ which is derived from J, the transition matrix of $\widetilde{M}$, in the following way. The set of vertices, $\widetilde{V}$, represents the states of $\widetilde{M}$, which is simply V. The edge set, $\widetilde{E}$, represents the possible transitions. The set of edge weights, $\widetilde{W}$, represents the transition probabilities. The idea is to partition $\widetilde{G}$ into subgraphs based on connectivity properties. We begin by placing all the vertices of $\widetilde{V}$ in a set C. The algorithm works by taking a vertex, s, of minimal vertex degree in C. It uses this vertex as the basis of a superstate S. The algorithm considers all vertices adjacent to S. For each adjacent vertex, s', if the subgraph of $\widetilde{G}$ formed by s' and S satisfies certain criteria, then s' is added to S. The process continues until no more vertices can be added to S. At that stage, the vertices in S are removed from C and classified as a superstate, and the algorithm begins again, considering the remaining unclassified vertices.

The criteria that the subgraph of $\widetilde{G}$ defined by the vertex set $\{s'\} \cup S$ must satisfy are the following.

1. Either a *completeness* criterion or a *fullness* criterion.
    (i) The completeness criterion requires that $\frac{\phi_{\{s'\} \cup S}}{\phi_S} > \alpha$ for some $\alpha > 0$, where ϕ_G is the ratio of the number of edges in the graph G to the number of edges that G would have if it were complete.
    (ii) The fullness criterion requires that s' be adjacent to at least a proportion β of vertices in S for some $\beta > 0$.
2. A *threshold* criterion. This requires that at least one transition probability from s' into a state in S be bigger than γ and that at least one transition probability from S to s' be bigger than γ for some $\gamma > 0$.

The algorithm can be summarized as follows.

ALGORITHM 3.2 (graph-theoretic decomposition of the jump chain).
1. *Put $C = V$. Set $j = 1$.*
2. *Put $S = S' = \emptyset$.*
3. *Choose from C a vertex s of minimal degree, mark it, and add it to S.*
4. *Move to S' all vertices adjacent to s.*
5. *Choose a vertex s' in S'.*
6. *If the fullness or connectivity criterion is satisfied and the threshold criterion is satisfied, then move s' to S and add to S' all vertices in C adjacent to s'. Otherwise, move s' to C.*
7. *If $S' \neq \emptyset$, repeat from step 5.*
8. *Put aside the vertices in S as superstate V_j.*
9. *If $C \neq \emptyset$, set $j = j + 1$, and repeat from step 2.*

We choose the parameters α, β, and γ so that the superstates are quite small but contain all problem regions. A discussion of how to choose these parameters is given in [5]. In practice, we try a number of different parameter combinations and choose

the one that gives the best tradeoff between performance (measured, for example, by the average amount of physical time achieved by the algorithm in a fixed number of steps) and fineness of segmentation. Note that the spatial extent of the superstates must be considerably smaller than the size of the observation window in order to avoid problems in calculating distances traveled by the random walker. To be more precise, in the following we assume that for every $j \in \{1, \ldots, \mathcal{L}\}$ there exists $s \in V_j$ with $\delta(s, s') \leq \min(a_x, a_y, a_z)/4$ for all $s' \in V_j$ and all s' adjacent to an element of V_j.

3.2.2. Aggregating the problem regions. Given a partition, $\{V_j\}_{j=1}^{\mathcal{L}}$, of the state space V, we calculate the expected time spent in each superstate and the transition probabilities from superstates to adjacent superstates. These quantities are dependent not only on the current superstate but also on the state (in the original state space) from which it was entered. Thus, in order to retain the Markov property, we adopt a finer state space than $\{V_j\}_{j=1}^{\mathcal{L}}$. We define our state space to be the states on the boundaries of the superstates. We call these states the *outer states* and denote them by $\mathring{V} \subset V$. More precisely, a state $s \in V_j$ is contained in $\mathring{V}$ if and only if there exists $s' \in V \setminus V_j$ such that M can move from s to s' with a positive transition rate. We are able to model the random walker as it moves from an outer state of one superstate to an outer state of another superstate in such a way that the process is Markovian and the expected times spent in superstates and transition probabilities between superstates can be calculated exactly.
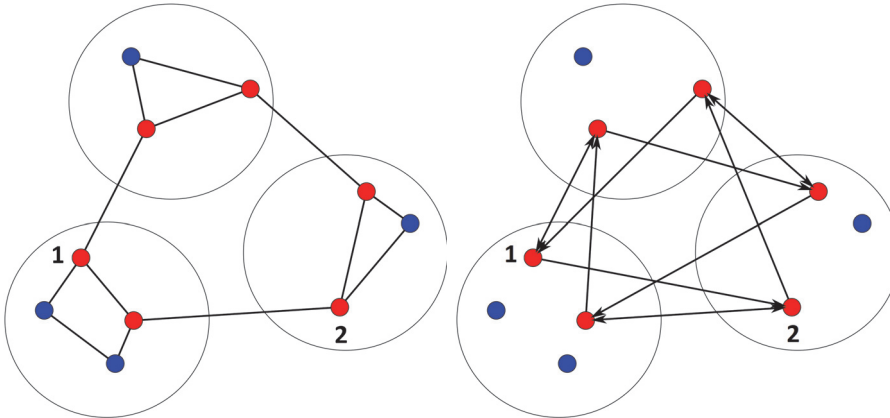

FIG. 3. *Left: Superstates, with outer states identified in red. Right: The possible transitions for the Markov chain on the outer states. Note that states 1 and 2 are not adjacent in the original state space V, but on $\mathring{V}$ they are.*

For each state $s \in \mathring{V}$ and each adjacent state $s' \in \mathring{V}$ of another superstate, we calculate $\mathring{p}_{s,s'}$, the probability of the walker moving from s to s', and $\mathring{\tau}_{s,s'}$, the expected time that the walker spends in the superstate before it moves from state s to state s'. Note that since we consider the transitions between superstates, in resolution of the outer states, s and s' can be adjacent although they are not adjacent in the original graph G (see also Figure 3). The quantities $\mathring{p}_{s,s'}$ and $\mathring{\tau}_{s,s'}$ are calculated by treating the states of a superstate as the transient states of an MJP, with the adjacent (outer) states acting as absorbing states. That is, for $j \in \{1, \ldots, \mathcal{L}\}$ we denote by V'_j the union of V_j and all outer states $\mathring{V}$ which can be reached from a state in V_j with positive probability. Then for each $j \in \{1, \ldots, \mathcal{L}\}$ we consider an

MJP $M^{(j)} = \{M_t^{(j)}\}_{t\geq 0}$ on the state space V_j' whose transition rates are determined as follows. The rate of moving from a state $s \in V_j$ to a state in $s' \in V_j'$ is given by the transition rate from state s to state s' in the original MJP M. Additionally, every state in $V_j' \setminus V_j$ is absorbing.

The transition probability from an outer state s to an adjacent outer state s' from a different superstate is then given by the probability of absorption in s', given that the MJP starts in s. This is calculated by considering the jump chain of $M^{(j)}$, where j corresponds to the superstate containing s. The transition matrix of the jump chain can be written in the form

$$(3.4) \qquad J^{(j)} = \begin{pmatrix} I & 0 \\ J^{(j),\text{TA}} & J^{(j),\text{TT}} \end{pmatrix},$$

where $J^{(j),\text{TA}}$ is the matrix of transition probabilities from transient states to absorbing states, $J^{(j),\text{TT}}$ is the matrix of transition probabilities from transient states to transient states, I is an identity matrix of appropriate size, and 0 is a matrix of zeros. The probability of absorption in state k', having begun in state k, is then given by $(\widetilde{P}^{(j)})_{k,k'}$, where $\widetilde{P}^{(j)} = (I - J^{(j),\text{TT}})^{-1} J^{(j),\text{TA}}$. The probability $\mathring{p}_{s,s'}$ is the element of this matrix where k corresponds to s and k' corresponds to s'.

The conditional expected time to absorption in state s' starting in state s can be calculated by considering the generator matrix of $M^{(j)}$, which can be written in the form

$$(3.5) \qquad Q^{(j)} = \begin{pmatrix} 0_1 & 0_2 \\ Q^{(j),\text{TA}} & Q^{(j),\text{TT}} \end{pmatrix}.$$

The matrix of conditional expected absorption times is given by $(\widetilde{\tau}^{(j)})_{k,k'} = \widetilde{T}_{k,k'}^{(j)}/\widetilde{P}_{k,k'}^{(j)}$, where $\widetilde{T}^{(j)} = ((Q^{(j),\text{TT}})^2)^{-1} Q^{(j),\text{TA}}$. The expected time $\mathring{\tau}_{s,s'}$ is the element of this matrix where k corresponds to s and k' corresponds to s'. Note that these expected times are then used in place of the exponentially distributed times used in the original MJP.

3.2.3. Simulating the random walk. Given an aggregation of the state space, we consider the Markov chain $\mathring{M} = \{\mathring{M}_n\}_{n\geq 0}$ on $\mathring{V}$ with $\mathring{\ell} = |\mathring{V}|$. We denote the transition matrix of $\mathring{M}$ by $\mathring{J} = (\mathring{p}_{s,s'})_{s,s'\in\mathring{V}}$, where $\mathring{p}_{s,s'} = 0$ when s and s' are not adjacent or are contained in the same superstate. The AMC estimator of the velocity is formally defined as

$$\widehat{\mathbf{v}_{\text{amc}}}(t) = \frac{1}{t} \sum_{i=0}^{\mathring{N}_t - 1} \mathbf{d}_{\mathring{M}_i, \mathring{M}_{i+1}},$$

where $\mathring{N}_t = \sup\{n \geq 0 : \sum_{i=0}^{n-1} \mathring{\tau}_{\mathring{M}_i, \mathring{M}_{i+1}} < t\}$. It is implemented as follows.

ALGORITHM 3.3 (aggregate Monte Carlo (AMC) estimation of velocity).
1. *Select $\mathring{M}_0$ uniformly from $1, \ldots, \mathring{\ell}$. Put $t = 0$ and $\mathbf{d} = \mathbf{0}$. Put $n = 0$.*
2. *Put $\mathring{M}_{n+1} = s$ with probability $\mathring{p}_{\mathring{M}_n, s}$.*
3. *Put $t = t + \mathring{\tau}_{\mathring{M}_n, \mathring{M}_{n+1}}$.*
4. *Put $\mathbf{d} = \mathbf{d} + \mathbf{d}_{\mathring{M}_n, \mathring{M}_{n+1}}$.*
5. *Put $n = n + 1$, and repeat from step 2 until $t > t_0$.*
6. *Return the estimator $\widehat{\mathbf{v}_{\text{amc}}}(t) = \mathbf{d}/t$.*

3.3. Asymptotic properties of the AMC estimator. In this section we prove a number of consistency results for the AMC estimators $\widehat{\mathbf{v}_{\mathsf{amc}}}(t)$. We again defer all proofs to the appendix.

THEOREM 3.2. *It holds that* $\lim_{t\to\infty} \widehat{\mathbf{v}_{\mathsf{amc}}}(t) = \tilde{\mathbf{v}}$ *a.s. and in* L^1, *where* $\tilde{\mathbf{v}}$ *is the limit considered in Theorem* 3.1.

Similarly to the approach used in section 3.1, it is convenient to consider an intermediate estimator $\{\mathbf{v}_{\mathsf{a},1}(t)\}_{t\geq 0}$ whose precise definition is given below. The proof of Theorem 3.2 is then subdivided into showing $\lim_{t\to 0} \widehat{\mathbf{v}_{\mathsf{cmc}}}(t) - \mathbf{v}_{\mathsf{a},1}(t) = 0$ a.s. on one hand and $\lim_{t\to 0} \widehat{\mathbf{v}_{\mathsf{amc}}}(t) - \mathbf{v}_{\mathsf{a},1}(t) = 0$ a.s. on the other. The L^1-convergence is an immediate consequence of the dominated convergence theorem, as $\widehat{\mathbf{v}_{\mathsf{amc}}}(t)$ is bounded from above by

$$\max_{s,s'\in\mathring{V}} \mathbf{d}_{s,s'} \Big/ \min_{\substack{s,s'\in\mathring{V} \\ \mathring{\tau}_{s,s'}>0}} \mathring{\tau}_{s,s'}.$$

To introduce the estimator $\{\mathbf{v}_{\mathsf{a},1}(t)\}_{t\geq 0}$ we make use of a coupling of $\mathring{M}$ and M in the sense that we define a Markov chain $\mathring{M}^c$ that is defined on the same probability space as the MJP M and has the same distribution as the Markov chain $\mathring{M}$; see Lemma B.1. The idea for defining $\mathring{M}^c$ is to trace the superstate transitions of the jump process $\widetilde{M}$, as illustrated in Figure 4.
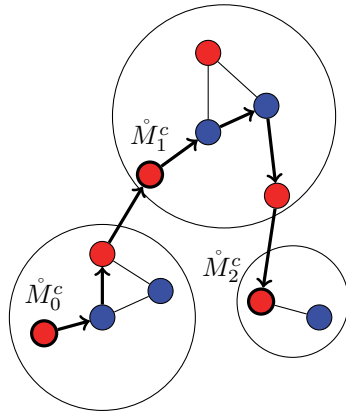

FIG. 4. *Possible trajectory of the random walker* M *with outer states identified in red. The highlighted states* $\mathring{M}_0^c, \mathring{M}_1^c, \mathring{M}_2^c$ *correspond to the outer states at which* M *enters a new superstate.*

In order to define $\mathring{M}^c$ precisely, we will need some notation that allows us to easily switch between the state space V associated with the CMC algorithm and the state space of $\mathring{V}$ associated with the AMC algorithm. For every $s \in V$ denote by $\sigma(s) \in \{V_1, \ldots, V_{\mathcal{L}}\}$ the superstate containing s. In order to convert the CMC time scale into the AMC time scale, we define a function $f_{\mathsf{ca}} : \mathbb{N}_0 \to \mathbb{N}_0$ by

$$f_{\mathsf{ca}}(n) = \left|\left\{i \in \{1, \ldots, n\} : \sigma\left(\widetilde{M}_i\right) \neq \sigma\left(\widetilde{M}_{i-1}\right)\right\}\right|,$$

where $\mathbb{N}_0 = \{0, 1, \ldots\}$ denotes the set of nonnegative integers; i.e., $f_{\mathsf{ca}}(n)$ counts the number of superstates visited by $\widetilde{M}$ in the first n steps. The function f_{ca} can also be considered as a random clock that advances every time a superstate transition is

observed and remains constant otherwise. Similarly, in order to convert the AMC timescale into the CMC timescale, we define a function $f_{\mathsf{ac}} : \mathbb{N}_0 \to \mathbb{N}_0$ by

$$f_{\mathsf{ac}}(n) = \inf \left\{ n' \geq 0 : f_{\mathsf{ca}}(n') = n \right\};$$

i.e., $f_{\mathsf{ac}}(n)$ denotes the number of steps performed by $\widetilde{M}$ at the time of the nth superstate transition. Thus, the function f_{ac} can also be considered as generalized inverse of the random clock f_{ca}. Using these definitions, we consider the process $\mathring{M}^c = \{\mathring{M}_n^c\}_{n \geq 0}$ given by $\mathring{M}_n^c = \widetilde{M}_{f_{\mathsf{ac}}(n)}$. We also put $\mathring{N}_t^c = f_{\mathsf{ca}}(N_t)$ and define the intermediate estimator

$$(3.6) \qquad\qquad \mathbf{v}_{\mathsf{a},1}(t) = \frac{1}{t} \sum_{i=0}^{\mathring{N}_t^c - 1} \mathbf{d}_{\mathring{M}_i^c, \mathring{M}_{i+1}^c}, \qquad t > 0,$$

where we show in Lemma B.2 that $\mathbb{P}\left(\lim_{t \to \infty} \widehat{\mathbf{v}_{\mathsf{cmc}}}(t) - \mathbf{v}_{\mathsf{a},1}(t) = 0\right) = 1$.

Finally, we consider the difference between $\mathbf{v}_{\mathsf{a},1}(t)$ and the AMC estimator $\widehat{\mathbf{v}_{\mathsf{amc}}}(t)$. Indeed,

$$
\begin{aligned}
|\widehat{\mathbf{v}_{\mathsf{amc}}}(t) - \mathbf{v}_{\mathsf{a},1}(t)| &= \frac{1}{t} \left| \sum_{n=0}^{\mathring{N}_t - 1} \mathbf{d}_{\mathring{M}_n^c, \mathring{M}_{n+1}^c} - \sum_{n=0}^{\mathring{N}_t^c - 1} \mathbf{d}_{\mathring{M}_n^c, \mathring{M}_{n+1}^c} \right| \\
&\leq \frac{1}{t} \left| \mathring{N}_t - \mathring{N}_t^c \right| (a_x + a_y + a_z),
\end{aligned}
$$

where in the equality we used the fact that the processes $\mathring{M}$ and $\mathring{M}^c$ have the same distribution; see Lemma B.1. Hence, the proof of Theorem 3.2 is completed once we show that

$$\mathbb{P}\left(\lim_{t \to \infty} \frac{1}{t} \left(\mathring{N}_t - \mathring{N}_t^c \right) = 0 \right) = 1.$$

This is done in Lemma B.3.

4. Application to DCV4T molecules. A major application of our framework is in describing charge transport in amorphous organic semiconductors, which are used in organic electronics. In this setting, the random environment represents a molecular morphology, and the random walker describes the movement of charges (holes or electrons). In general, organic electronic devices are built from organic semiconductors such as polymers or small molecules. Examples of organic electronic devices are organic solar cells and organic light emitting diodes. Organic solar cells are an alternative to classical silicon-based solar cells, as they are environmentally friendly and mechanically flexible. In order to build efficient organic electronic devices, it is important to understand elementary processes (e.g., charge transfer) within the device. It is important, for example, that holes and electrons (charges) traverse the network at a high velocity, measured via charge carrier mobility. In this section, we consider the problem of estimating the drift velocity or charge mobility of a weighted spatial graph corresponding to systems of DCV4T molecules. DCV4T is a small molecule used as an electron-donor in organic solar cells; see Figure 5 for its chemical structure. To increase the understanding of charge transport processes in organic semiconductors, there are several physical modeling approaches, one of which is microscopic simulation. Here, a large-scale molecular morphology is simulated using

molecular dynamics, and the network of molecules is represented as a spatial graph, where the vertices correspond to centers of mass of molecules and edges to possible transitions between neighboring molecules; see Figure 1 (right). Transition or hopping rates are determined using first principles calculations. In this section, we fit the stochastic morphology model introduced in section 2 to a realization of a DCV4T graph obtained using microscopic simulation.
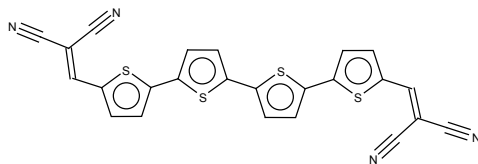

Fig. 5. *Molecular structure of DCV4T.*

4.1. Microscopic simulation. We briefly summarize how the molecular morphology of an amorphous system of DCV4T molecules is obtained by microscopic simulation. An example of such a morphology is given on the left-hand side in Figure 1. The extracted graph is given on the right-hand side. For general information on the microscopic approach, see [20], where a large-scale morphology of Alq3 molecules is simulated. For specific details on the microscopic simulation of DCV4T, we refer the reader to [10, 23, 24].

The microscopic model is constructed in two stages. In the first stage, a spatial graph is obtained which represents the molecular morphology. This is achieved by simulating an amorphous morphology of 4096 DCV4T molecules using atomistic molecular dynamics. As an initial configuration, the molecules are placed on a cubic lattice. Then, this system of molecules is equilibrated for 10 ns using molecular dynamics well above the glass transition temperature, 800 K. This system is then quenched (i.e., cooled down) to room temperature. The centers of mass of the molecules for a given snapshot define the vertices of the graph. An edge is placed between two vertices if the distance between any of the thiophene or dicyanovinyl groups is less than a threshold of 0.8 nm (see [24]).

In the second stage, the transfer rates between neighboring molecules are determined. For neighboring molecules, transition rates (i.e., charge hopping rates) are calculated using the Marcus transfer rate equation, given as (2.4), with the pair-specific quantities (the reorganization energy λ_{ij}, the electronic coupling element $\mathcal{J}_{ij}$, and the site-energy η_i) determined using electronic structure techniques, polarizable force-field methods, or a combination of both (see [4, 9, 20]).

For DCV4T, the reorganization energy of 0.21 eV was used for all molecules. Electronic coupling elements $\mathcal{J}_{ij}$ are calculated for each pair of neighboring molecules based on the semiempirical ZINDO approach as implemented in the Molecular Orbital Overlap module of the VOTCA package (see [13, 20]). Site energies η_i are calculated by using the Thole model (see [28]) as implemented in the VOTCA package (see [20]).

The result of the microscopic approach is a weighted spatial graph $G^{\mathsf{Mol}} = (V^{\mathsf{Mol}}, E^{\mathsf{Mol}}, W^{\mathsf{Mol}})$ in a bounded observation window $A \subset \mathbb{R}^3$. The set of vertices V^{Mol} describes the positions of the centers of masses of the DCV4T molecules. The set of edges E^{Mol} describes those pairs of vertices (i.e., pairs of centers of masses of molecules) between which charge transfer is sufficiently likely. Charges can only make transitions along the edges of the graph. The edge weights W^{Mol} give the transition

rates between neighboring vertices. Note that the resulting graph is connected and that all distances are determined using cyclic boundary conditions; see section 2.1.

4.2. Model fitting and validation of the random spatial graph. We fit the parameters of the random spatial graph model, $G = (V, E, W)$, introduced in section 2, to a system of DCV4T molecules gained by microscopic simulation, as explained in section 4.1. We make use of fitting techniques similar to those described in [2]. To begin with, the parameters of the dominance-competition model representing the vertex model are fitted to the set of vertices V^{Mol} of the microscopic simulation.
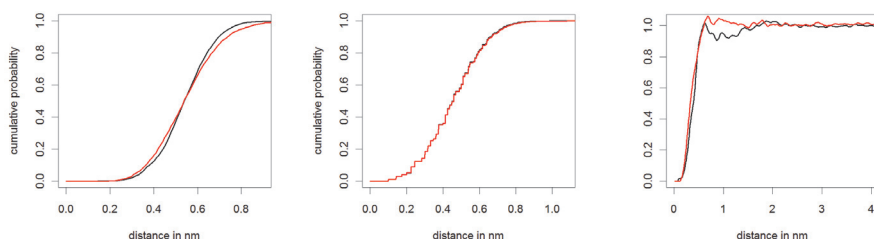

Fig. 6. *Nearest neighbor distance distribution function (left), spherical contact distribution function (center), and pair-correlation function (right) for vertices obtained using the microscopic approach (black) and vertices from the corresponding realization of the stochastic model (red).*

We use the minimum contrast method (see, e.g., [1]) to fit the parameters of our vertex model. The parameters are chosen to minimize the discrepancy between the estimated nearest neighbor distance distribution functions of the microscopic model's vertices and the points of the dominance-competition process; see Figure 6 (left). The nearest neighbor distance distribution function $D(r)$ gives the probability that the nearest neighbor of a randomly chosen vertex is within distance r. To check if the set of vertices V^{Mol} of the microscopic simulation is adequately represented by the stochastic vertex model, the point patterns are visually compared to each other in Figure 7, where a very good agreement is found. For a more formal model validation, we compute further structural characteristics for the vertex set V^{Mol} and realizations of the dominance-competition process; see Figure 6 (center and right). In particular, we compute the spherical contact distribution function $H : [0, \infty) \to [0, 1]$, where the value $H(r)$ describes the probability of reaching a vertex from a randomly chosen point in the observation window within distance r and the pair-correlation function $g : [0, \infty) \to [0, \infty)$, where the value $g(r)$ is proportional to the relative frequency of point pairs with distance r. For both characteristics a reasonable agreement is found; see Figure 6.

The fitting technique for the vertex marks and edge weights of the random graph is the same as that described in [2]. We give here only a brief summary. The marks of the vertices are fitted using the minimum contrast method with the mark-correlation function as the summary statistic. Maximum likelihood as well as least-squares are used to fit the remaining parameters to the observed edge weights of the microscopic simulation. The good fit of the mark-correlation functions (which were used for model fitting) is evident in Figure 8 (left).

To fit the edge model of the random spatial graph to the edge set E^{Mol} of the microscopic simulation, the values of r_{min} and r_{max} are estimated by the minimum and maximum edge lengths observed in the edge set E^{Mol}. Furthermore, we estimate
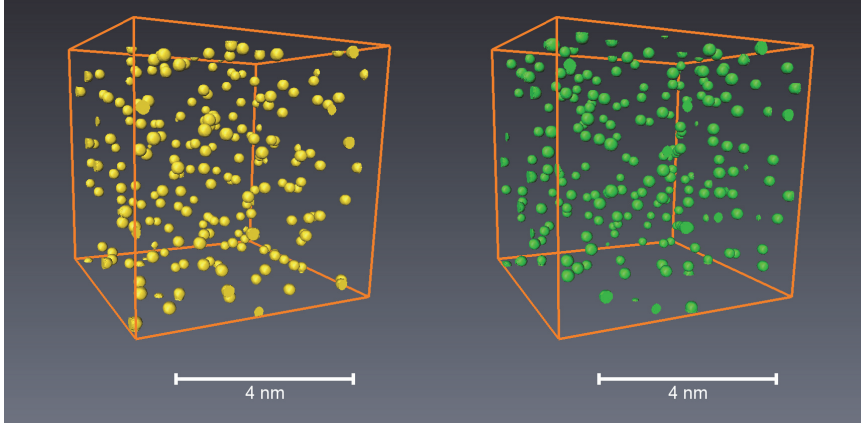
FIG. 7. *Left: 3D vertices obtained using the microscopic approach (cut-out) and a realization of the fitted stochastic point-process model (right).*

d_min as the minimum vertex degree observed in E^Mol. Choosing $c = 7$ yields an average vertex degree $d_\mathsf{mean} = 17.4$ for the stochastic model which can be compared to $d^\mathsf{Mol}_\mathsf{mean} = 17.0$ for the microscopic model. The function $f : [0, \infty) \to [0, 1]$ introduced in section 2.3 is described by a piecewise polynomial of the form

$$f(r) = \begin{cases} 1 & \text{for } r \leq r_\mathsf{min}, \\ a_1 r^2 + a_2 r + a_3 & \text{for } r_\mathsf{min} < r \leq r_\mathsf{max}, \\ 0 & \text{else,} \end{cases}$$

whose parameters a_1, a_2, and a_3 are fitted to match the trend of decreasing edge putting probabilities observed in G^Mol; see also Figure 8 (right). The edge length distributions of E^Mol and the edge model match very well (see Figure 8, center). The visual agreement between the stochastic graph and the microscopic counterpart is also very good; see Figure 9.
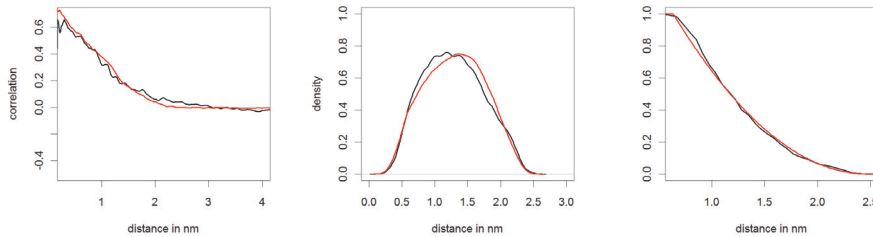

FIG. 8. *Left: Mark-correlation function. Center: Density of edge lengths. The black curves indicate the microscopic approach and the red curves the stochastic model. Right: Edge connection probability estimated from the microscopic model (black) and fitted polynomial function f (red).*

The transition rates depend on the energies associated with each vertex, $\{\eta_i\}_{i=1}^\ell$, and the transfer integrals, $\{\mathcal{J}_{ij}\}_{i=1,j=1,i\neq j}^{\ell,\ell}$. The general procedure for generating these quantities is described in section 2.4. Before generating the energies, we use minimum contrast estimation to find the parameters of the energy model, $\mu_\eta = -1.99\mathrm{eV}$, $\sigma_\eta^2 = 0.064\mathrm{eV}^2$, $\omega = 0.21$, and $k = 15$.
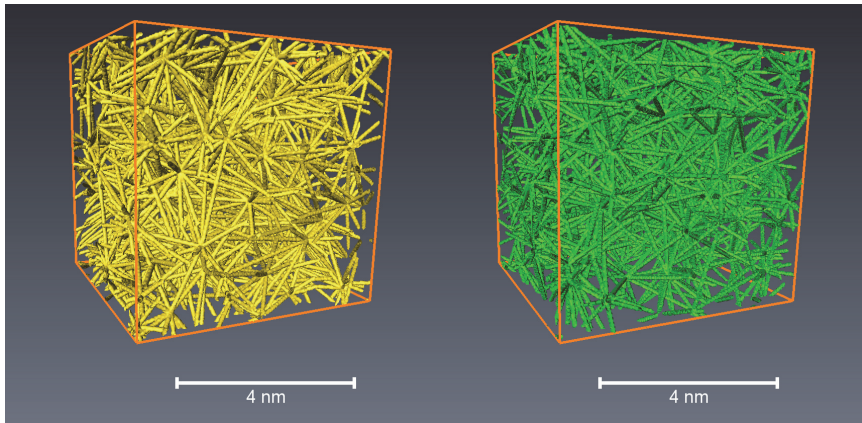
FIG. 9. *3D graph by microscopic approach (left, cut-out) and a realization of the fitted stochastic model (right).*

Analysis of the distributions of transfer integrals $\{\mathcal{J}_{ij}\}_{i=1,j=1,i\neq j}^{\ell,\ell}$ for all pairs of neighboring molecules of the microscopic model shows that $\log_{10}(\mathcal{J}_{ij}^2)$ is Gaussian distributed for molecules whose distance, r, is within a certain fixed interval, with mean and variance of the Gaussian distribution changing with distance; see Figures 10(a) and (b). This effectively takes into account the interplay between the anisotropy of a single DCV4T molecule and the amorphous morphology. After determining the pairwise distance dependence from the microscopic model, values are drawn following a Gaussian distribution with the appropriate parameters. Figure 10(c) shows the overall frequency of rates after entering site positions, energies, and electronic couplings.
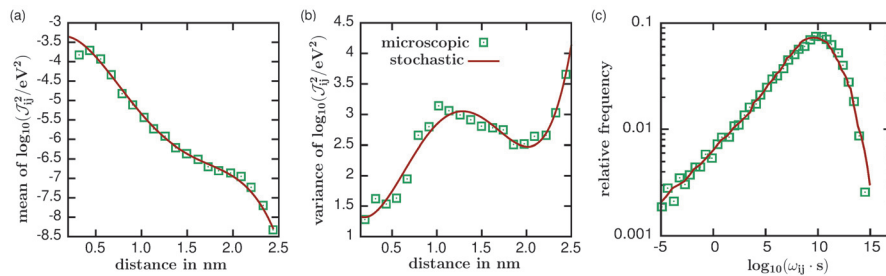

FIG. 10. *Left: Comparison of mean values of $\log_{10}(\mathcal{J}_{ij}^2)$ for the microscopic and stochastic models. Center: Comparison of variances of $\log_{10}(\mathcal{J}_{ij}^2)$ for the microscopic and stochastic models. Right: Comparison of relative frequencies of transition rates for the stochastic and microscopic models.*

Both the microscopic model G^{Mol} and the random 3D graph model G are constructed in order to estimate the charge mobility in amorphous semiconductors. To check if the fitted random graph model G describes the reference graph G^{Mol} adequately, we calculate the charge mobility for both models and compare the obtained results. Note that the mobility $\mathbf{v}/|\mathbf{F}|$, being the quotient of charge velocity $\mathbf{v}$ and strength of the electric field $|\mathbf{F}|$, is a 3D vector. Since the mobility is only nonzero in the direction of the electric field electric $\mathbf{F}$, we consider $\zeta = \mathbf{v}^{\mathsf{T}}\mathbf{F}/|\mathbf{F}|^2$, the mobility in the direction of the electric field.

In Figure 11, we show the mobilities versus field as computed from G^{MOL} (the microscopic model) and G (the stochastic model). We first ignore the site-energy disorder; i.e., we put $\Delta\eta_{ij}^{\mathsf{el}} = 0$ in the expression for the rates in (2.4). In the upper panel of Figure 11, one can see that the absolute values and a slight decrease with the increasing field strength (inverted regime) are similar for both models. Taking the energetic disorder into account (lower panel) reduces the value of mobility by seven orders of magnitude and is due to large disorder in site-energies. Again, both models agree almost perfectly. Note that the mobility is rather sensitive to deviations in the model. If, for instance, the distances between vertices are too large, this will result in much lower squared electronic coupling elements and, consequently, lower mobilities. Thus, the presented stochastic model offers a good description of molecular networks in amorphous semiconductors.
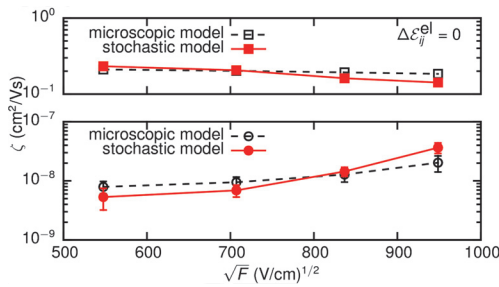

FIG. 11. *Average hole mobilities $\overline{\zeta}$ (in direction of the electric field) in dependence of the electric field for stochastic model (red; averaged over five realizations) and microscopic model (black; averaged over six different field directions and five injection points).*

4.3. Numerical results. One of the primary strengths of our RWRE approach to the modeling of charge transport properties is that it allows for the fast generation of different realizations of the stochastic network. It also allows for much larger models than those generated using molecular simulation. To demonstrate the flexibility of our RWRE approach, we generated ten realizations of the stochastic DCV4T model in a bounded region $A = [0, a_x] \times [0, a_y] \times [0, a_z]$, with $a_x = a_y = a_z \approx 13.71$nm. Each of these realizations consists of approximately 4000 molecules. We then considered the effect of increasing system size. We did this by considering systems with five and ten times greater volume. That is, we generated realizations in the bounded regions $A_5 = [0, 5^{1/3}a_x] \times [0, 5^{1/3}a_y] \times [0, 5^{1/3}a_z]$ and $A_{10} = [0, 10^{1/3}a_x] \times [0, 10^{1/3}a_y] \times [0, 10^{1/3}a_z]$.

For each of these realizations, we calculated the mobility, ζ, along the x direction, $\zeta = \mathbf{v}^{\mathsf{T}}\mathbf{F}/|\mathbf{F}|^2$, where $\mathbf{F} = F\mathbf{e}$, $F = |\mathbf{F}|$, and $\mathbf{e} = (1, 0, 0)^{\mathsf{T}}$ for a number of different values of F (Poole–Frenkel dependence).

We used the AMC algorithm to estimate the mobilities for the various sizes of the observation window. The segmentation of the state space V was carried out with parameters $\alpha = \beta = .2$ and $\gamma = .02$. These values were chosen based on the numerical study done in [5]. In the case of the systems in A and A_5, we ran the algorithm for approximately 2.1×10^9 steps. In the case of the system in A_{10} we ran the simulation for 6.3×10^9 steps. These values were chosen using some pilot runs in order to ensure that the estimates were sufficiently accurate. We report the average mobilities $\overline{\zeta}$ over all realizations of each system size in Table 1. We include the standard errors of the estimates of the average mobilities.

As one can see, the average mobility decreases by several orders of magnitude once

Average mobilities and standard errors (S.E.) for realizations of $DCV4T$ systems in A, A_5, and A_{10}.

Force ($V/$cm).	A $\overline{\zeta}$ (S.E.)	A_5 $\overline{\zeta}$ (S.E.)	A_{10} $\overline{\zeta}$ (S.E.)
1×10^5	2.1×10^{-9} (6.4×10^{-10})	1.0×10^{-10} (4.8×10^{-11})	3.8×10^{-11} (1.6×10^{-11})
2×10^5	4.1×10^{-8} (1.5×10^{-9})	1.4×10^{-10} (8.2×10^{-11})	3.8×10^{-11} (1.7×10^{-11})
3×10^5	6.4×10^{-9} (2.4×10^{-9})	6.2×10^{-11} (2.0×10^{-11})	4.8×10^{-11} (2.4×10^{-11})
4×10^5	9.5×10^{-9} (3.4×10^{-9})	9.9×10^{-11} (4.9×10^{-11})	6.0×10^{-11} (1.5×10^{-11})
5×10^5	1.5×10^{-8} (5.2×10^{-9})	2.9×10^{-10} (2.1×10^{-10})	6.9×10^{-11} (2.2×10^{-11})
6×10^5	2.5×10^{-8} (8.4×10^{-9})	3.2×10^{-10} (1.8×10^{-10})	9.3×10^{-11} (3.3×10^{-11})
7×10^5	3.5×10^{-8} (1.3×10^{-8})	5.7×10^{-10} (3.2×10^{-10})	1.3×10^{-10} (4.6×10^{-11})
8×10^5	4.5×10^{-8} (1.89×10^{-8})	9.6×10^{-10} (4.8×10^{-10})	1.9×10^{-10} (6.3×10^{-11})
9×10^5	5.6×10^{-8} (2.5×10^{-8})	1.5×10^{-9} (6.6×10^{-10})	1.9×10^{-10} (7.2×10^{-11})

the system size is increased; see also Figure 12. This is a typical indication of a finite size effect observed when simulating drift-diffusion in systems with rough energetic landscapes (see [14]). The reason for this is that periodic (cyclic) boundary conditions are used to mimic infinitely large systems. Therefore, statistical averages are performed over limited subsets of distributions available in the periodically replicated box. This results in, for example, larger average energy of a particle as compared to an infinitely large system. In other words, the random walker has a higher effective temperature and therefore drift-diffuses with a higher mobility.

The finite size effects are logarithmic in system size; i.e., the transition between so-called dispersive and nondispersive transport occurs for ℓ which exponentially grows with the square of energetic disorder in units of k_BT (see [3, 14]). It is therefore very important to use adequate system sizes in order to make accurate estimates of nondispersive mobilities. This can be achieved by constructing coarse-grained stochastic models and combining them with the AMC scheme, as presented here.

5. Conclusions. In this paper, we proposed a general toolkit for the study of the charge transport properties of materials via random walks in random environments (RWRE). In particular, we presented a flexible stochastic model for disordered media: a random spatial graph model with directed edge weights, where the edge weights represented the transition rates of a Markov jump process (MJP) modeling the motion of the random walker. We described the AMC estimator to efficiently estimate the random walker's velocity by Monte Carlo simulations. We proved the strong consistency of the AMC velocity estimator. Thereafter, we applied the presented toolbox for a detailed case study describing the motion of holes in a network of DCV4T molecules. In particular, we analyzed the system-size dependency of the hole's velocity and mobility, respectively.
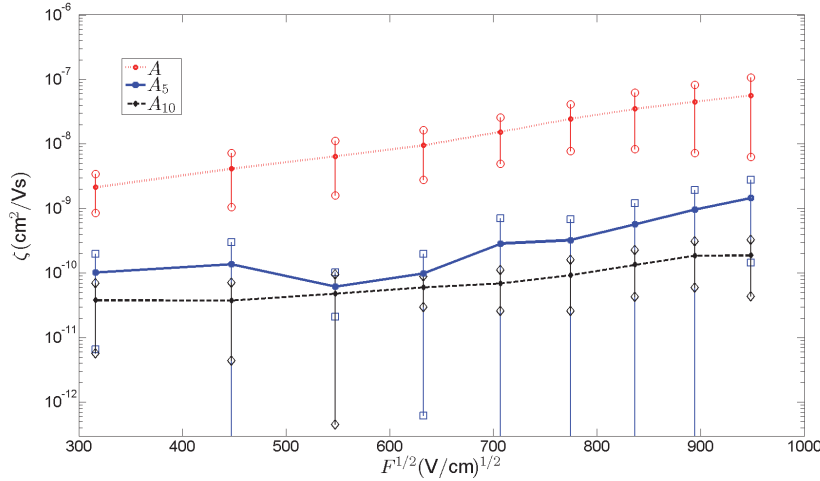
FIG. 12. *Poole–Frenkel plot of the average mobilities for the various system sizes with error bars showing ± 2 S.E.*

Appendix.

A. Proof of Theorem 3.1. First, we provide details concerning the proof of Theorem 3.1. Note that $\widehat{\mathbf{v}_{\mathsf{cmc}}}(t)$ admits the representation

$$\widehat{\mathbf{v}_{\mathsf{cmc}}}(t) = \frac{1}{t} \sum_{s,s' \in V} N_{s,s'}(t) \mathbf{d}_{s,s'},$$

where $N_{s,s'}(t)$ denotes the number of times the MJP M jumps from state s to state s' before time t.

That is, for $s, s' \in V$, $N_{s,s'}(t) = |\{n \in \{0, \ldots, N_t - 1\} : \widetilde{M}_n = s, \widetilde{M}_{n+1} = s'\}|$.

LEMMA A.1. *It holds that $\mathbb{P}\left(\lim_{t \to \infty} (\widehat{\mathbf{v}_{\mathsf{cmc}}}(t) - \mathbf{v}_{\mathsf{c},1}(t)) = 0\right) = 1$.*

Proof. First, note that

$$\widehat{\mathbf{v}_{\mathsf{cmc}}}(t) - \mathbf{v}_{\mathsf{c},1}(t) = \sum_{s,s' \in V} \left(\frac{N_{s,s'}(t)}{T_{s,s'}(t)} - q_{s'} \right) \frac{T_{s,s'}(t) \mathbf{d}_{s,s'}}{t}.$$

As $T_{s,s'}(t)/t$ is bounded from above by 1, it suffices to show

$$(\text{A.1}) \qquad \mathbb{P}\left(\lim_{t \to \infty} \frac{T_{s,s'}(t)}{N_{s,s'}(t)} = \frac{1}{q_{s'}} \right) = 1.$$

To prove (A.1) we note that $T_{s,s'}(t) - \sum_{i=1}^{N_{s,s'}(t)-1} \sigma_i$ is contained in the interval $[0, \sigma_{N_{s,s'}(t)}]$, where the sequence $(\sigma_i)_{i \geq 1}$ is defined by

$$\sigma_i = \sup_{t \geq 0} \left\{ \left| \{n \in \{0, \ldots, N_t\} : \widetilde{M}_{n-1} = s, \widetilde{M}_n = s'\} \right| = i \right\}$$

$$- \inf_{t \geq 0} \left\{ \left| \{n \in \{0, \ldots, N_t\} : \widetilde{M}_{n-1} = s, \widetilde{M}_n = s'\} \right| = i \right\}.$$

In other words, σ_i denotes the waiting time at node s' when it is visited for the ith time coming from state s. By the Markovian structure of M, the times $(\sigma_i)_{i \geq 1}$ form

independent $\mathsf{Exp}(q_{s'})$ distributed variables so that (A.1) follows from the law of large numbers. □

Finally, the following uniform integrability result implies L^1-convergence.

LEMMA A.2. *The family of random variables $\{\widehat{\mathbf{v}_{\mathsf{cmc}}}(t)\}_{t\geq 0}$ is uniformly integrable.*

Proof. We construct a family $\{\mathbf{v}(t)\}_{t\geq 0}$ of L^1-convergent random variables such that $\widehat{\mathbf{v}_{\mathsf{cmc}}}(t)$ is a.s. bounded from above by $\mathbf{v}(t)$. Put $q_0 = \max_{s\in V} q_s$. When conditioning the waiting times $\{T_n\}_{n\geq 0}$ associated with the MJP M on the jump chain $\widetilde{M}$, they form a sequence of independent and exponentially distributed variables, where the parameter of the nth waiting time is given by $q_{\widetilde{M}_n}$. In particular, there exists a sequence $\{T_n^{(1)}\}_{n\geq 0}$ of (unconditionally) independent and exponentially distributed random variables such that $T_n^{(1)} \leq T_n$ a.s. and such that $T_n^{(1)}$ is exponentially distributed with parameter q_0. Writing $N_t^{(1)} = \sup\{n \geq 0 : \sum_{i=0}^{n-1} T_i^{(1)} < t\}$, we therefore obtain $\widehat{\mathbf{v}_{\mathsf{cmc}}}(t) \leq \mathbf{v}(t)$, where $\mathbf{v}(t) = \frac{1}{t} N_t^{(1)} (a_x, a_y, a_z)^\top$. Since the random variables $N_t^{(1)}/t$ converge to $1/q_0$ in L^1, this completes the proof of Lemma A.2. □

B. Proof of Theorem 3.2. In this section, we provide the proofs for the results given in section 3.3. In the following, for ease of presentation, it is convenient to assume that $\widetilde{M}_0 \in \mathring{V}$. The reader will have few difficulties in modifying the subsequent arguments for the general case.

LEMMA B.1. *The processes $\mathring{M}$ and $\mathring{M}^c$ have the same distribution.*

Proof. It suffices to show that the conditional distribution of the random variable $\mathring{M}_n^c$ given $\mathring{M}_1^c, \ldots, \mathring{M}_{n-1}^c$ depends only on $\mathring{M}_{n-1}^c$ and equals the conditional distribution of $\mathring{M}_n$ given $\mathring{M}_{n-1}$. Since $\mathring{M}_{n-1}^c = \widetilde{M}_{f_{\mathsf{ac}}(n-1)}$ and since $\mathring{M}_1^c, \ldots, \mathring{M}_{n-1}^c$ are measurable with respect to $\widetilde{M}_0, \widetilde{M}_1, \ldots, \widetilde{M}_{f_{\mathsf{ac}}(n-1)}$, we can further reduce the problem to identifying the conditional distribution of $\mathring{M}_n^c$ given $\widetilde{M}_0, \widetilde{M}_1, \ldots, \widetilde{M}_{f_{\mathsf{ac}}(n-1)}$. More precisely, we show

$$(B.1) \qquad \mathbb{P}\left(\mathring{M}_n^c = s' \mid \widetilde{M}_{f_{\mathsf{ac}}(n-1)} = s, \widetilde{M}_{f_{\mathsf{ac}}(n-1)-1}, \ldots, \widetilde{M}_0\right) = \mathring{p}_{s,s'}$$

for all $i \in \{1, \ldots, \mathcal{L}\}$, $s \in \mathring{V} \cap V_i$, and $s' \in \mathring{V} \setminus V_i$. The strong Markov property implies that the left-hand side of (B.1) equals the probability that the MJP M started at s exits the corresponding superstate $\sigma(s)$ via s'. But by definition, the latter probability is just $\mathring{p}_{s,s'}$. □

Next, we compare the asymptotic behavior of $\widehat{\mathbf{v}_{\mathsf{cmc}}}(t)$ and $\mathbf{v}_{\mathsf{a},1}(t)$.

LEMMA B.2. *It holds that $\mathbb{P}\left(\lim_{t\to\infty} \widehat{\mathbf{v}_{\mathsf{cmc}}}(t) - \mathbf{v}_{\mathsf{a},1}(t) = 0\right) = 1$.*

Proof. Let $i \in \{1, \ldots, \mathring{\ell}\}$ be arbitrary. From our assumption (see section 3.2.1) that there exists $s_0 \in V_i'$ such that $\delta(s, s_0) \leq \min(a_x, a_y, a_z)/4$ we deduce $\mathbf{d}_{s,s'} + \mathbf{d}_{s',s''} = \mathbf{d}_{s,s''}$ for all $s, s', s'' \in V_i'$. In particular,

$$(B.2) \qquad \mathbf{d}_{\mathring{M}_j^c, \mathring{M}_{j+1}^c} = \sum_{n=f_{\mathsf{ac}}(j)}^{f_{\mathsf{ac}}(j+1)-1} \mathbf{d}_{\widetilde{M}_n, \widetilde{M}_{n+1}}$$

for all $j \in \{0, \ldots, \mathring{N}_t^c - 1\}$, so that summing over $j \in \{0, \ldots, \mathring{N}_t^c - 1\}$ yields

$$
\widehat{\mathbf{v_{cmc}}}(t) = \frac{1}{t} \sum_{n=0}^{f_{ac}(\mathring{N}_t^c)-1} \mathbf{d}_{\widetilde{M}_n, \widetilde{M}_{n+1}} + \frac{1}{t} \sum_{n=f_{ac}(\mathring{N}_t^c)}^{N_t-1} \mathbf{d}_{\widetilde{M}_n, \widetilde{M}_{n+1}}
$$

$$
= \frac{1}{t} \sum_{n=0}^{\mathring{N}_t^c-1} \mathbf{d}_{\mathring{M}_n^c, \mathring{M}_{n+1}^c} + \frac{1}{t} \mathbf{d}_{\widetilde{M}_{f_{ac}(\mathring{N}_t^c)}, \widetilde{M}_{N_t}},
$$

where (B.2) has been used in the last equality. From $\widetilde{M}_{f_{ac}(\mathring{N}_t^c)}, \widetilde{M}_{N_t} \in A$ we conclude that $|\mathbf{d}_{\widetilde{M}_{f_{ac}(\mathring{N}_t^c)}, \widetilde{M}_{N_t}}| \le a_x + a_y + a_z$. Thus the assertion follows. $\qquad \square$

Finally, our last result concerns the comparison of the asymptotic behavior of $\mathring{N}_t$ and $\mathring{N}_t^c$.

LEMMA B.3. *It holds that* $\lim_{t \to \infty} t^{-1}(\mathring{N}_t - \mathring{N}_t^c) = 0$ *a.s.*

Proof. This auxiliary result is proven by showing that both $\mathring{N}_t/t$ and $\mathring{N}_t^c/t$ converge a.s. to the same deterministic value $1/b$, where

$$
b = \sum_{s \in \mathring{V}} \mu_s \sum_{\substack{s' \in \mathring{V} \\ \mathring{p}_{s,s'} > 0}} \mathring{p}_{s,s'} \mathring{\tau}_{s,s'},
$$

and $(\mu_s)_{s \in \mathring{V}}$ denotes the stationary limit distribution of the Markov chain $\mathring{M}^c$. For $s, s' \in \mathring{V}$ with $\mathring{p}_{s,s'} > 0$ and $n_1, n_2 \ge 0$ with $n_1 \le n_2$ we say that $F = \{n_1, n_1 + 1, \ldots, n_2\}$ forms an (s, s')-excursion if $\widetilde{M}_{n_1} = s$, $\widetilde{M}_{n_2+1} = s'$, and $\widetilde{M}_k \in \sigma(s)$ for all $k \in \{n_1, \ldots, n_2\}$. The family of all (s, s')-excursions is denoted by $F_{s,s'}$. Similarly, for $s \in \mathring{V}$ we put $F_s = \bigcup_{s' \in V} F_{s,s'}$. For $n \ge 0$ and $s, s' \in V$ we write $F_{s,s'}(n)$ for the set of all $F \in F_{s,s}$ satisfying $F \subset \{0, \ldots, f_{ac}(n) - 1\}$. Furthermore, for $n \ge 0$ and $s \in \mathring{V}$ we denote by $N_s(n) = |\{i \in \{0, \ldots, n\} : \mathring{M}_i^c = s\}|$ the number of visits in the state $s \in \mathring{V}$ during the first n steps of the Markov chain $\mathring{M}^c$. Then

$$
1 \ge \limsup_{t \to \infty} \frac{1}{t} \sum_{n=0}^{N_t-1} T_n
$$

$$
\ge \limsup_{t \to \infty} \frac{\mathring{N}_t^c}{t} \sum_{s \in V'} \frac{N_s(\mathring{N}_t^c)}{\mathring{N}_t^c} \sum_{\substack{s' \in V \\ \mathring{p}_{s,s'} > 0}} \frac{|F_{s,s'}(\mathring{N}_t^c)|}{N_s(\mathring{N}_t^c)} \frac{\sum_{F \in F_{s,s'}(\mathring{N}_t^c)} \sum_{k \in F} T_k}{|F_{s,s'}(\mathring{N}_t^c)|},
$$

where in the second inequality we decompose the path of the particle into its (s, s')-excursions. Note that this inequality is strict if M_t is not an outer state. Next, we determine the asymptotic behavior of the fractions appearing in the latter expression. As $\widetilde{M}$ forms a Markov chain, for every $s, s' \in \mathring{V}$ with $\mathring{p}_{s,s'} > 0$ the sequences $\{(\widetilde{M}_k, T_k)\}_{k \in F}$, $F \in F_{s,s'}$ are independent and identically distributed (iid). In particular, the random variables $\sum_{k \in F} T_k$, $F \in F_{s,s'}$ form iid copies of the time to absorption of the particle started at s and conditioned to be absorbed in s'. Since $\mathring{N}_t^c \to \infty$ a.s. as $t \to \infty$, the law of large numbers yields

$$
\mathbb{P}\left(\lim_{t \to \infty} \frac{\sum_{F \in F_{s,s'}(\mathring{N}_t^c)} \sum_{k \in F} T_k}{|F_{s,s'}(\mathring{N}_t^c)|} = \mathring{\tau}_{s,s'} \right) = 1.
$$

Similarly, for every $s \in \mathring{V}$ the sequences $\{\widetilde{M}_k\}_{k \in F}$, $F \in F_s$ are iid, and for every $s' \in V$, $F \in F_s$ the indicator $\mathbf{1}_{F \in F_{s,s'}}$ constitutes a Bernoulli random variable with success probability $\mathring{p}_{s,s'}$. Therefore, another application of the law of large numbers shows that

$$\mathbb{P}\left(\lim_{t \to \infty} \frac{\left|F_{s,s'}(\mathring{N}_t^c)\right|}{N_s\left(\mathring{N}_t^c\right)} = \mathring{p}_{s,s'}^c\right) = 1.$$

Finally, an application of the ergodic theorem for the Markov chain $\mathring{M}^c$ (see [19, Theorem 1.10.2]) yields

$$\mathbb{P}\left(\lim_{t \to \infty} \frac{N_s(\mathring{N}_t^c)}{\mathring{N}_t^c} = \mu_s\right) = 1.$$

Hence, we obtain $\limsup_{t \to \infty} \mathring{N}_t^c/t \leq 1/b$. Very similar arguments can be used to show that $\liminf_{t \to \infty} \mathring{N}_t^c/t \geq 1/b$ a.s., but for the convenience of the reader we provide some of the details. Indeed, noting

$$1 \leq \liminf_{t \to \infty} \frac{1}{t} \sum_{n=0}^{N_t} T_n$$

$$\leq \liminf_{t \to \infty} \frac{\mathring{N}_t^c + 1}{t} \sum_{s \in \mathring{V}} \frac{N_s\left(\mathring{N}_t^c + 1\right)}{\mathring{N}_t^c + 1} \sum_{\substack{s' \in V \\ \mathring{p}_{s,s'} > 0}} \frac{\left|F_{s,s'}(\mathring{N}_t^c + 1)\right|}{N_s\left(\mathring{N}_t^c + 1\right)} \frac{\sum_{F \in F_{s,s'}(\mathring{N}_t^c+1)} \sum_{k \in F} T_k}{\left|F_{s,s'}(\mathring{N}_t^c + 1)\right|}$$

$$= \left(\liminf_{t \to \infty} \mathring{N}_t^c/t\right) b$$

completes the proof of $\mathbb{P}(\lim_{t \to \infty} \mathring{N}_t^c/t = b^{-1}) = 1$. To show $\mathbb{P}(\lim_{t \to \infty} \mathring{N}_t/t = 1/b) = 1$ we may proceed similarly. Indeed, with probability 1,

$$1 \geq \limsup_{t \to \infty} \frac{1}{t} \sum_{j=0}^{\mathring{N}_t - 1} \mathring{\tau}_{\mathring{M}_j, \mathring{M}_{j+1}}$$

$$\geq \limsup_{t \to \infty} \frac{\mathring{N}_t}{t} \sum_{s \in \mathring{V}} \frac{N_s\left(\mathring{N}_t\right)}{\mathring{N}_t} \sum_{\substack{s' \in V \\ \mathring{p}_{s,s'} > 0}} \frac{\left|F_{s,s'}\left(\mathring{N}_t\right)\right|}{N_s\left(\mathring{N}_t\right)} \mathring{\tau}_{s,s'},$$

where in the second inequality we again decompose the path of the particle into its (s, s')-excursions. This yields $\mathbb{P}(\limsup_{t \to \infty} \mathring{N}_t/t \leq 1/b) = 1$. Finally,

$$1 \leq \liminf_{t \to \infty} \frac{1}{t} \sum_{j=0}^{\mathring{N}_t} \mathring{\tau}_{\mathring{M}_j, \mathring{M}_{j+1}}$$

$$\leq \liminf_{t \to \infty} \frac{\mathring{N}_t + 1}{t} \sum_{s \in \mathring{V}} \frac{N_s\left(\mathring{N}_t + 1\right)}{\mathring{N}_t + 1} \sum_{\substack{s' \in V \\ \mathring{p}_{s,s'} > 0}} \frac{\left|F_{s,s'}\left(\mathring{N}_t + 1\right)\right|}{N_s\left(\mathring{N}_t + 1\right)} \mathring{\tau}_{s,s'},$$

so that $\mathbb{P}(\liminf_{t \to \infty} \mathring{N}_t/t \geq 1/b) = 1$. $\square$

REFERENCES

[1] A. J. Baddeley, *Spatial point processes and their applications*, in Stochastic Geometry, W. Weil, ed., Springer, Berlin, 2007, pp. 1–75.

[2] B. Baumeier, O. Stenzel, C. Poelking, D. Andrienko, and V. Schmidt, *Stochastic modeling of molecular charge transport networks*, Phys. Rev. B, 86 (2012), 184202.

[3] P. M. Borsenberger, E. H. Magin, M. Der VanAuweraer, and F. C. De Schryver, *The role of disorder on charge transport in molecularly doped polymers and related materials*, Physica Status Solidi A, 140 (1993), pp. 9–47.

[4] J. L. Brédas, D. Beljonne, V. Coropceanu, and J. Cornil, *Charge-transfer and energy-transfer processes in Pi-Conjugated oligomers and polymers: A molecular picture*, Chem. Rev., 104 (2004), pp. 4971–5004.

[5] T. Brereton, O. Stenzel, B. Baumeier, D. Andrienko, V. Schmidt, and D. P. Kroese, *Efficient simulation of Markov chains using segmentation*, Methodol. Comput. Appl. Probab., 16 (2014), pp. 465–484.

[6] T. Brereton, O. Stenzel, B. Baumeier, V. Schmidt, and D. P. Kroese, *Efficient simulation of charge transport in deep-trap media*, in Proceedings of the 2012 Winter Simulation Conference (Berlin, Germany, 2012), C. Laroque, J. Himmelspach, R. Pasupathy, O. Rose, and A. M. Uhrmacher, eds., IEEE, Washington, DC, 2012. DOI: 10.1109/WSC.2012.6465003.

[7] S. N. Chiu, D. Stoyan, W. S. Kendall, and J. Mecke, *Stochastic Geometry and Its Applications*, 3rd ed., J. Wiley & Sons, Chichester, 2013.

[8] H. Choi and D. B. Szyld, *Application of threshold partitioning of sparse matrices to Markov chains*, in Proceedings of the IEEE International Computer Performance and Dependability Symposium, IPDS'96, IEEE Computer Society, Los Alamitos, CA, 1996, pp. 158–165.

[9] V. Coropceanu, J. Cornil, D. A. da Silva Filho, Y. Olivier, R. Silbey, and J. L. Brédas, *Charge transport in organic semiconductors*, Chem. Rev., 107 (2007), pp. 926–952.

[10] C. Elschner, M. Schrader, R. Fitzner, A. A. Levin, P. Baeuerle, D. Andrienko, K. Leo, and M. Riede, *Molecular ordering and charge transport in a dicyanovinyl-substituted quaterthiophene thin film*, RSC Adv., 3 (2013), pp. 12117–12123.

[11] B. D. Hughes, *Random Walks and Random Environments. Volume 2: Random Environments*, Oxford University Press, New York, 1996.

[12] A. P. J. Jansen, *An Introduction to Kinetic Monte Carlo Simulations of Surface Reactions*, Springer, New York, 2012.

[13] J. Kirkpatrick, *An approximate method for calculating transfer integrals based on the ZINDO Hamiltonian*, Internat. J. Quantum Chem., 108 (2008), pp. 51–56.

[14] A. Lukyanov and D. Andrienko, *Extracting nondispersive charge carrier mobilities of organic semiconductors from simulations of small systems*, Phys. Rev. B, 82 (2010), 193202.

[15] R. A. Marcus, *Electron transfer reactions in chemistry. Theory and experiment*, Rev. Modern Phys., 65 (1993), p. 599.

[16] F. May, M. Al-Helwi, B. Baumeier, W. Kowalsky, E. Fuchs, C. Lennartz, and D. Andrienko, *Design rules for charge-transport efficient host materials for phosphorescent organic light-emitting diodes*, J. Amer. Chem. Soc., 134 (2012), pp. 13818–13822.

[17] F. May, B. Baumeier, C. Lennartz, and D. Andrienko, *Can lattice models predict the density of states of amorphous organic semiconductors?*, Phys. Rev. Lett., 109 (2012), 136401.

[18] B. Movaghar, B. Pohlmann, and W. Schirmacher, *Theory of electronic hopping transport in disordered materials*, Philosophical Magazine Part B, 41 (1980), pp. 49–63.

[19] J. R. Norris, *Markov Chains*, Cambridge University Press, Cambridge, UK, 1998.

[20] V. Rühle, A. Lukyanov, F. May, M. Schrader, T. Vehoff, J. Kirkpatrick, B. Baumeier, and D. Andrienko, *Microscopic simulations of charge transport in disordered organic semiconductors*, J. Chem. Theory Comput., 7 (2011), pp. 3335–3345.

[21] H. Scher and M. Lax, *Stochastic transport in a disordered solid. I. Theory*, Phys. Rev. B, 7 (1973), pp. 4491–4502.

[22] H. Scher and E. W. Montroll, *Anomalous transit-time dispersion in amorphous solids*, Phys. Rev. B, 12 (1975), pp. 2455–2477.

[23] M. Schrader, R. Fitzner, M. Hein, C. Elschner, B. Baumeier, M. Riede, K. Leo, P. Baeuerle, and D. Andrienko, *Comparative study of microscopic charge dynamics in crystalline acceptor-substituted oligothiophenes*, J. Amer. Chem. Soc., 134 (2012), pp. 6052–6056.

[24] M. Schrader, C. Korner, C. Elschner, and D. Andrienko, *Charge transport in amorphous and smectic mesophases of dicyanovinyl-substituted oligothiophenes*, J. Materials Chem., 22 (2012), pp. 22258–22264.

[25] W. J. Stewart, *Introduction to the Numerical Solution of Markov Chains*, Princeton University Press, Princeton, NJ, 1994.

[26] D. Stoyan, *Thinnings of point processes and their use in the statistical analysis of a settlement pattern with deserted villages*, Statistics, 19 (1988), pp. 45–56.

[27] N. Tessler, Y. Preezant, N. Rappaport, and Y. Roichman, *Charge transport in disordered organic materials and its relevance to thin-film devices: A tutorial review*, Adv. Materials, 21 (2009), pp. 2741–2761.

[28] B. T. Thole, *Molecular polarizabilities calculated with a modified dipole interaction*, Chem. Phys., 59 (1981), pp. 341–350.

[29] J. J. M. van der Holst, F. W. A. van Oost, R. Coehoorn, and P. A. Bobbert, *Monte Carlo study of charge transport in organic sandwich-type single-carrier devices: Effects of Coulomb interactions*, Phys. Rev. B, 83 (2011), 085206.

[30] P. H. Wang, R. B. Best, and J. Blumberger, *Multiscale simulation reveals multiple pathways for $H2$ and $O2$ transport in a [NiFe]-Hydrogenase*, J. Amer. Chem. Soc., 133 (2011), pp. 3548–3556.

[31] O. Zeitouni, *Random walks in random environment*, in Lectures on Probability Theory and Statistics, J. Picard, ed., Springer, Berlin, 2004, pp. 189–312.